

Iowa State University

From the Selected Works of Cameron A. MacKenzie

May, 2013

Extremes of Nonlinear Vibration: Comparing Models Based on Moments, L-Moments, and Maximum Entropy

Steven R. Winterstein
Cameron A. MacKenzie



Available at: https://works.bepress.com/cameron_mackenzie/4/

Extremes of Nonlinear Vibration: Comparing Models Based on Moments, L-Moments, and Maximum Entropy

Steven R. Winterstein

Principal Engineer
Probability-Based Engineering,
Menlo Park, CA
e-mail: SteveWinterstein@alum.mit.edu

Cameron A. MacKenzie

Assistant Professor
Naval Postgraduate School,
Monterey, CA
e-mail: cmackenzie@ou.edu

Wind and wave loads on offshore structures show nonlinear effects, which require non-Gaussian statistical models. Here we critically review the behavior of various non-Gaussian models. We first survey moment-based models; in particular, the four-moment “Hermite” model, a cubic transformation often used in wind and wave applications. We then derive an “L-Hermite” model, an alternative cubic transformation calibrated by the response “L-moments” rather than its ordinary statistical moments. These L-moments have recently found increasing use, in part because they show less sensitivity to distribution tails than ordinary moments. We find here, however, that these L-moments may not convey sufficient information to accurately estimate extreme response statistics. Finally, we show that four-moment maximum entropy models, also applied in the literature, may be inappropriate to model broader-than-Gaussian cases (e.g., responses to wind and wave loads). [DOI: 10.1115/1.4007050]

Introduction

Nonlinear effects beset virtually all aspects of offshore structural loading and response. These nonlinearities cause non-Gaussian statistical effects, which are often most consequential in the extreme events—e.g., 100- to 10,000-year conditions—that govern structural reliability. Thus there is engineering interest in forming accurate non-Gaussian models of time-varying loads and responses, and calibrating them from the limited data at hand.

Our goal here is to critically assess the accuracy of different non-Gaussian models. In particular, two comparisons are considered:

1. Models based on moments versus L-moments.
2. Moment-based models based on (Hermite) transformations versus maximum entropy.

Comparison 1 is motivated by the increasing use of L-moments [1] in offshore engineering; e.g., for wave runup [2] and Morison drag [3]. This comparison is made with “Hermite” models, which assume the non-Gaussian response $x(t)$ is a cubic (Hermite) transformation, either to or from a Gaussian process $u(t)$ [4,5]. While Hermite models based on traditional moments are well-known, those based on L-moments are newly derived here. It is shown here, however, that these L-moments may not convey sufficient information to accurately estimate extreme response statistics.

Comparison 2 considers how moments—which are found superior to L-moments in the information they convey about extremes—are optimally used. Specifically, Hermite models are compared with four-moment maximum entropy models, also widely applied in the literature (e.g., [6,7]). While based on the same moment information, these models may show quite different tail behavior. In particular, it is found that maximum entropy may be inappropriate to model broader-than-Gaussian cases (e.g., responses to wind and wave loads).

Finally, note that many of our results—e.g., Figs. 2–9—use examples that are largely academic (though the polynomial model in Figs. 2–5 may represent a quadratic or higher-order drag

effect). This is to permit comparison with exact results, and thus promote critical understanding of the accuracy of the different methods. The last example (Fig. 10) is an actual wind loading example, often studied in the probabilistic mechanics community (e.g., [8,9]). Note too that we have found similar conclusions when comparing these models to field measurements of North Sea current speeds [10].

General Results for L-Moments

Due to their relative novelty, the properties of L-moments are first surveyed. This section closely follows the work of Hosking [1], where much additional information can be found. Perhaps the simplest way to view L-moments is in terms of an ordered sample of size n ($X_{1:n} \leq X_{2:n} \leq \dots \leq X_{n:n}$) drawn from the distribution of X . The n th L-moment λ_n is then defined as a linear combination of the order statistics $E[X_{i:n}]$. In particular, the first four L-moments are

$$\lambda_1 = E[X] \quad (1)$$

$$\lambda_2 = \frac{1}{2}E[X_{2:2} - X_{1:2}] \quad (2)$$

$$\lambda_3 = \frac{1}{3}E[X_{3:3} - 2X_{2:3} + X_{1:3}] \quad (3)$$

$$\lambda_4 = \frac{1}{4}E[X_{4:4} - 3X_{3:4} + 3X_{2:4} - X_{1:4}] \quad (4)$$

Clearly λ_1 and λ_2 are measures of central trend and dispersion. Higher L-moments reflect different aspects of distribution shape. In terms of the CDF of X , $F(x) = P[X \leq x]$, or its inverse $x(F)$, λ_3 and λ_4 reflect the second and third derivatives of these functions (in a finite difference sense). If X is uniformly distributed on $[0,1]$, these functions are linear, $E[X_{i:n}] = i/(n+1)$, and hence $\lambda_n = 0$ for $n \geq 3$. Nonzero $\lambda_3, \lambda_4, \dots$ reflect deviations of the distribution of X from a uniform density: λ_3 and λ_4 reflect asymmetric and symmetric deviations, respectively. Thus, the unitless quantities $\tau_3 = \lambda_3/\lambda_2$ and $\tau_4 = \lambda_4/\lambda_2$ have come to be known, respectively, as the L-skewness and L-kurtosis.

From the distribution theory of the order statistics $X_{i:n}$, Eqs. (1)–(4) can be rewritten in terms of either $F(x)$ or $x(F)$:

Contributed by the Ocean Offshore and Arctic Engineering Division of ASME for publication in the JOURNAL OF OFFSHORE MECHANICS AND ARCTIC ENGINEERING. Manuscript received July 14, 2011; final manuscript received April 13, 2012; published online February 25, 2013. Assoc. Editor: Bernt J. Leira.

$$\lambda_n = \int_{F=0}^{F=1} x(F)w_n(F)dF = \int_{x=-\infty}^{x=+\infty} x \cdot w_n[F(x)]f(x)dx \quad (5)$$

in which $f(x) = dF/dx$ is the probability density of X . The weight functions here (w_n) are polynomial functions of F . In particular, the first four L-moments use the following weight functions:

$$w_1(F) = 1 \quad (6)$$

$$w_2(F) = 2F - 1 \quad (7)$$

$$w_3(F) = 6F^2 - 6F + 1 \quad (8)$$

$$w_4(F) = 20F^3 - 30F^2 + 12F - 1 \quad (9)$$

To estimate L-moments from a data set of size N , it is convenient to first sort the data into an ordered array $x_1 \leq x_2 \leq \dots \leq x_N$. The n th L-moment can then be estimated as

$$\hat{\lambda}_n = \frac{1}{N} \sum_{i=1}^N x_i w_n(\hat{F}_i) \quad (10)$$

Here \hat{F}_i is the estimated CDF value associated with x_i ; e.g., $\hat{F}_i = i/N$. One may instead use other “plotting point” locations of the general form $\hat{F}_i = (i + \gamma)/(N + \delta)$ for $\delta > \gamma > -1$.

L-Moments for Gaussian Variables. Consider now the special case of a standard normal variable, commonly denoted U , with cumulative distribution function $F(u) = \Phi(u)$ and probability density function $\phi(u) = \exp(-u^2/2)/\sqrt{2\pi}$. From Eq. (5) its L-moments are of the form

$$\lambda_n = \int_{u=-\infty}^{u=+\infty} u \cdot w_n[\Phi(u)]\phi(u)du = E\{Uw_n[\Phi(U)]\} \quad (11)$$

Because $w_1(u)$ and $w_3(u)$ are even functions of u , $uw_1(u)$ and $uw_3(u)$ are odd so that $\lambda_1 = \lambda_3 = 0$ in Eq. (11). The nonzero L-moments λ_2 and λ_4 are evaluated to be

$$\lambda_2[U] = \frac{1}{\sqrt{\pi}} = 0.56419, \quad \lambda_4[U] = 0.06917 \quad (12)$$

The corresponding L-skewness and L-kurtosis, $\tau_3 = \lambda_3/\lambda_2$ and $\tau_4 = \lambda_4/\lambda_2$, are then

$$\tau_3 = 0, \quad \tau_4 = \frac{0.06917}{0.56419} = 0.1226 \quad (13)$$

From Eq. (11) note that $\lambda_n = E[Uw_n(\Phi(U))]$, the expected product of U and the weight function $w_n(\Phi(U))$. Figure 1 shows the behavior of this product $L_n(u) = uw_n(\Phi(u))$ for $n=3$ and 4. It is clear that $L_n(u)$, and hence λ_n , gives much less weight to tail values than u^3 and u^4 , the weighting functions for standard moments of orders 3 and 4.

In particular, in the tails the weight functions in Eqs. (6)–(9) approach 1 in absolute value, so that extreme outcomes are weighed roughly linearly by the L-moments, rather than to the third and fourth powers by skewness and kurtosis. {This is sensible in that L-moments are linear combinations of order statistics—hence their name—and, unlike $\mu_n = E[(X - m_X)^n]$, all L-moments retain the units of X .} This tail insensitivity of L-moments will be shown below to be a drawback when one fits models to these moments to estimate extremes.

Transformation Models 1: Hermite Models

Hermite models are transformations of the form $X = g(U)$, in which g is a cubic function rearranged in terms of the Hermite polynomials $\text{He}_2(U) = U^2 - 1$ and $\text{He}_3(U) = U^3 - 3U$:

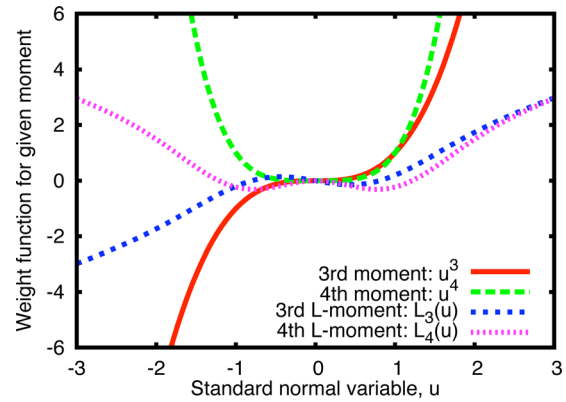


Fig. 1 Weight functions $L_n(u)$ contributing to the L-moment $\lambda_n = E[L_n(U)]$ for a standard normal variable U . Note lesser weight to extreme outcomes (large $|u|$) for λ_n than for ordinary moment $E[U^n]$.

$$X = m_X + \sigma_X \kappa [U + c_3(U^2 - 1) + c_4(U^3 - 3U)] \quad (14)$$

in which U is standard normal, and m_X and σ_X^2 are the mean and variance of X . We consider here only “softening” cases, whose kurtosis α_4 exceeds 3, the value in the Gaussian case. (For “hardening” cases in which $\alpha_4 < 3$, the roles of X and U are interchanged, using the cubic transformation to expand the tails of X to achieve Gaussianity. We believe this use of dual models greatly enhances modeling flexibility.)

By using Hermite polynomials in Eq. (14), the quantity in square brackets has zero mean and uncorrelated terms. Its variance is then $1 + c_3^2 E[\text{He}_2(U)^2] + c_4^2 E[\text{He}_3(U)^2]$, or simply $1 + 2c_3^2 + 6c_4^2$. Thus, ensuring Eq. (14) to have consistent variance requires

$$\kappa = \frac{1}{\sqrt{1 + 2c_3^2 + 6c_4^2}} \quad (15)$$

It remains to select the constants c_3 and c_4 to be consistent with the skewness α_3 and kurtosis α_4 of X . This is the topic of the remainder of this section.

Consider first the case in which $c_3 = 0$, so that X is symmetrically distributed about its mean. Its kurtosis in this case is

$$\alpha_4 = \frac{E[(X - m_X)^4]}{\sigma_X^4} = \frac{3 + 24c_4 + 252c_4^2 + 1296c_4^3 + 3348c_4^4}{(1 + 6c_4^2)^2} \quad (16)$$

Equation (16) gives an implicit result for c_4 , the cubic coefficient required to match the kurtosis α_4 found from a given model or data set. For small deviations from Gaussianity, c_4 will be small and explicit approximations for c_4 are possible. The simplest, “first-order” result retains only linear terms in c_4 from Eq. (16):

$$\alpha_4 = 3 + 24c_4, \quad c_4 = \frac{\alpha_4 - 3}{24} \quad (17)$$

The more standard, “second-order” Hermite model more accurately captures kurtosis by also retaining quadratic terms in c_4 (in both numerator and denominator of Eq. (16)):

$$\alpha_4 = 3 + 24c_4 + 216c_4^2, \quad c_4 = \frac{\sqrt{1 + 1.5(\alpha_4 - 3)} - 1}{18} \quad (18)$$

The effect of skewness is reflected in Eq. (14) through nonzero c_3 value. The (second-order) Hermite model uses the c_3 value

Table 1 Coefficients proposed for Eqs. (20) and (21) in [13]

Coefficients in Eqs. (20) and (21)			
	Equation (20)	Equation (21)	Equation (21)
p_1	0.1967	-0.0721	p_{10} 1.497×10^{-5}
p_2	-1.646×10^{-2}	3.176×10^{-2}	p_{11} 5.457×10^{-7}
p_3	1.809×10^{-2}	-2.942×10^{-2}	p_{12} 6.049×10^{-9}
p_4	7.438×10^{-4}	-1.790×10^{-3}	
p_5	-9.209×10^{-4}	2.348×10^{-3}	
p_6	-1.366×10^{-5}	5.965×10^{-5}	
p_7	1.527×10^{-4}	-6.282×10^{-4}	
p_8	1.070×10^{-5}	-6.355×10^{-5}	
p_9	8.823×10^{-8}	-9.692×10^{-7}	

$$c_3 = \frac{\alpha_3}{6(1 + 6c_4)} = \frac{\alpha_3}{4 + 2\sqrt{1 + 1.5(\alpha_4 - 3)}} \quad (19)$$

Equations (18) and (19), together with Eqs. (14) and (15), form the basis of the standard, second-order Hermite model.

Most recently, numerical routines are used (e.g., [11]) to obtain “exact” c_3 and c_4 values from constrained optimization, minimizing errors in matching moments while requiring that the Hermite transformation remains monotonic. (Newton-Raphson techniques have also been suggested [12] to estimate c_3 and c_4 .) Commonly these routines yield the specified moments to the tolerance requested. These are the source of the Hermite results shown here. Note too (e.g., for spreadsheets) that polynomials have recently been fit [13] to these exact c_3, c_4 values:

$$\frac{c_3}{\alpha_3} = p_1 + p_2\alpha_4 + p_3\alpha_3^2 + p_4\alpha_4^2 + p_5\alpha_3^2\alpha_4 + p_6\alpha_4^3 + p_7\alpha_3^4 + p_8\alpha_3^2\alpha_4^2 + p_9\alpha_4^4 \quad (20)$$

$$c_4 = p_1 + p_2\alpha_4 + p_3\alpha_3^2 + p_4\alpha_4^2 + p_5\alpha_3^2\alpha_4 + p_6\alpha_4^3 + p_7\alpha_3^4 + p_8\alpha_3^2\alpha_4^2 + p_9\alpha_4^4 + p_{10}\alpha_3^4\alpha_4 + p_{11}\alpha_3^2\alpha_4^3 + p_{12}\alpha_4^5 \quad (21)$$

Table 1 lists the p_i values. Within the region where Eq. (14) remains monotone—roughly, where $\alpha_4 \geq 3 + (1.25\alpha_3)^2$ —Eqs. (20) and (21) yield fitted R^2 values of 0.9988 and 0.9994, respectively [13].

Transformation Models 2: L-Hermite Models

We now seek to derive new models, again adopting a cubic Hermite transformation (Eq. (14)) now calibrated by L-moments. To calculate L-moments of Eq. (14), it is first useful to rearrange terms. Regrouping $U + c_4(U^3 - 3U)$ as $(1 - 3c_4)U + c_4U^3$ and dividing by $(1 - 3c_4)$, one finds the equivalent representation

$$X = m_X + K[U + b(U^2 - 1) + cU^3] \quad (22)$$

The benefit here is that the highest-order term is simplified to U^3 . To preserve the variance σ_X^2 , the scaling factor K now becomes

$$K = \frac{\sigma_X}{\sqrt{1 + 2b^2 + 6c + 15c^2}} \quad (23)$$

In terms of the original coefficients c_3 and c_4 , the new coefficients are $b = c_3/(1 - 3c_4)$ and $c = c_4/(1 - 3c_4)$.

Our goal now is to calibrate Eq. (22); i.e., choose b and c that yield a specified set of (τ_3, τ_4) values. Appendix 1 of [14] shows that this leads to the results

$$b = \frac{9.21\tau_3}{11.68 - 2.5\gamma}, \quad c = \frac{\gamma - 1}{11.68 - 2.5\gamma}, \quad \gamma = \frac{\tau_4}{\tau_{4,\text{Gauss}}} \quad (24)$$

in which $\tau_{4,\text{Gauss}} = 0.1226$ (Eq. (13)).

Equations (22)–(24) comprise the L-moment version of the Hermite model—referred to below as the “L-Hermite” model. The simplicity of these results is notable. The central moments $\mu_n = E[(X - m_X)^n]$ of Eq. (14) yield coupled results: both μ_3 and μ_4 vary with both c_3 and c_4 . This leads to approximate results for these coefficients (Eqs. (18) and (19)), and hence an analytical Hermite model that may only approximately match the desired skewness and kurtosis. In contrast, the L-moments of the Hermite model decouple: λ_3 depends only on b in Eq. (22), while λ_4 depends only on c . The results (Eq. (24)) permit the L-Hermite model to preserve the L-moment ratios τ_3 and τ_4 without approximation.

Example 1: Symmetric Transformations

We first consider $X(t)$ as a symmetric transformation of a standard normal process $U(t)$:

$$X(t) = g(U(t)) = U(t) + c|U(t)|^{m-1}U(t), \quad m = 2, 3, 4, \dots \quad (25)$$

For fluid loads, the quadratic case ($m=2$) corresponds to the standard Morison drag load model. Higher m values reflect higher-order models.

In general, the index m controls the tail behavior of X : $|X|$ grows like $|U|^m$ for large $|U|$. The coefficient c determines the relative importance of this nonlinear term; i.e., where in the distribution tails this term begins to dominate. For given m , the shape parameter c can be related to either the kurtosis α_4 or the L-kurtosis τ_4 . Such results are derived in appendix 1 of [14].

Our main goal here is to represent any symmetric nonlinear system by either its kurtosis α_4 or its L-kurtosis τ_4 . It is thus useful to compare different models, calibrated to have the same fourth moment or L-moment, to see what variability remains. We hope this remaining variability to be small; that is, that the fourth moment goes a long way toward “explaining” the tail behavior of a nonlinear system, regardless of the precise form of its nonlinearity.

Figures 2 and 3 show that for kurtosis-based models, this is generally the case. These show the mean upcrossing rate of $X(t)$, $\nu(x)$, for the various transformed Gaussian models in Eq. (25) with $m=2$ through 5 (denoted “quadratic” through “quintic”). In general, for any transformed Gaussian process $X(t) = g(U(t))$ we find

$$\nu(x) = \nu_0 \exp[-u^2(x)/2], \quad u(x) = g^{-1}(x) = \Phi^{-1}[F(x)] \quad (26)$$

Here ν_0 is the upcrossing rate of the median of $X(t)$, and F is the CDF of $X(t)$. All models in these figures have been calibrated—that is, their c values chosen—to have a specific kurtosis value: $\alpha_4 = 5$ in Fig. 2 and $\alpha_4 = 7$ in Fig. 3. (Numerical results in these figures use Eq. (26), and normalize x by its standard deviation σ_X .)

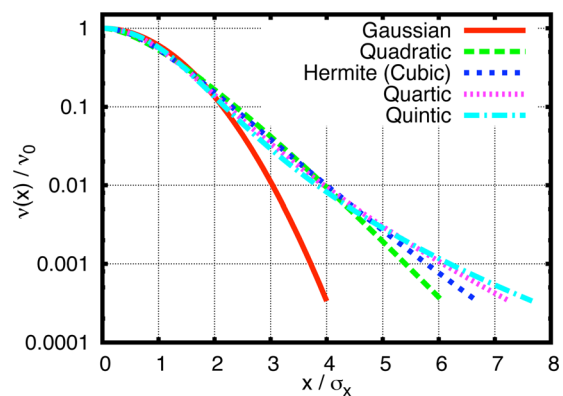


Fig. 2 Mean upcrossing rates for various transformed Gaussian models, all calibrated to have kurtosis $\alpha_4 = 5$

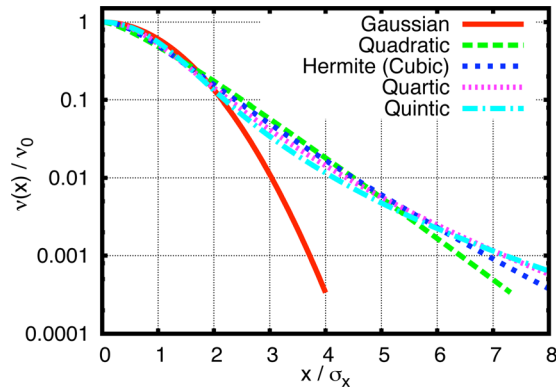


Fig. 3 Mean upcrossing rates for various transformed Gaussian models, all calibrated to have kurtosis $\alpha_4 = 7$

Note also that the cubic model coincides here, by definition, with the Hermite model.)

As may be expected, these models eventually diverge, and models of higher order (larger m) have PDFs with broader tails, and hence higher rates of upcrossings. Nonetheless, by preserving the fourth moment, the models cluster notably, yielding similar results to rates of about $\nu(x)/\nu_0 = 10^{-3}$. This is particularly significant because there are on the order of 1000 cycles in a typical stationary, 3-hour seastate (number of 10-s waves in 3 hours = 1080). Thus, four-moment models appear here to describe the tails sufficiently for practical purposes of extreme value analysis of marine structures.

In contrast, models fit here to L-moments do not define the response tails with comparable accuracy. Figures 4 and 5 show similar upcrossing rates, now found by preserving the fourth L-moment τ_4 . Specifically, these results use the values $\tau_4 = 0.185$ and 0.220, which are roughly consistent with the cubic model when $\alpha_4 = 5$ and 7, respectively. Thus, the results for the cubic model in Figs. 4 and 5 are similar to those in Figs. 2 and 3.

Most notably, different models with the same τ_4 yield markedly different tail behavior, exhibited here at crossing rates of about $\nu(x)/\nu_0 = 10^{-2}$. Thus, the benefit of L-moments—their tail insensitivity—is also their weakness: model uncertainty here begins to arise an order of magnitude more frequently—at levels crossed every 100 cycles rather than 1000—compared to four-moment Hermite models.

In concluding this example, we consider the expected fatigue damage $E[D]$ produced by these nonlinear loads. Because $E[D]$ is an integrated property, one may imagine that L-moment models can yield greater accuracy in these applications. As shown in the Appendix, however, L-moment models show similar inconsistencies in

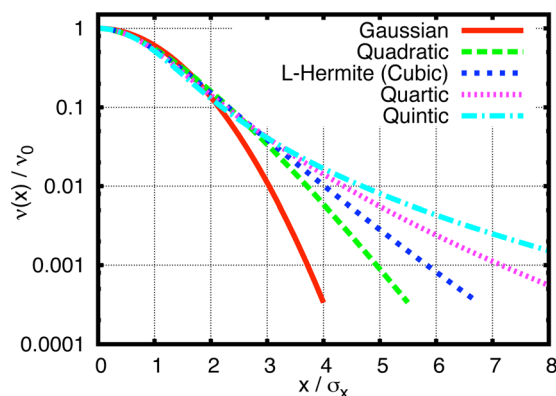


Fig. 4 Mean upcrossing rates for various transformed Gaussian models, all calibrated to have L-kurtosis $\tau_4 = 0.185$

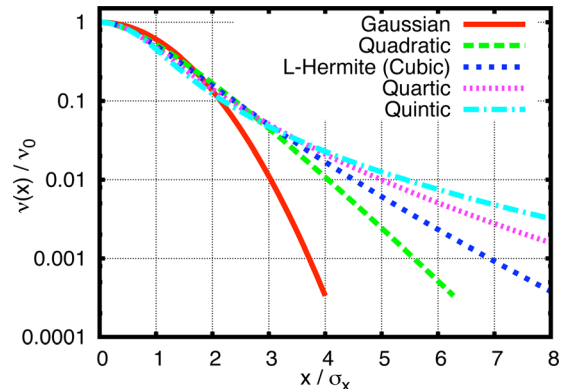


Fig. 5 Mean upcrossing rates for various transformed Gaussian models, all calibrated to have L-kurtosis $\tau_4 = 0.220$

fatigue predictions (Figs. 13 and 14 versus Figs. 11 and 12), again due to their relative tail insensitivity.

Example 2: Lognormal Models

To test asymmetric cases we consider the lognormal process $X(t)$ for which

$$X(t) = g(U(t)) = x_{.50} \exp[\sigma_{\ln X} U(t)], \quad \sigma_{\ln X}^2 = \ln(1 + V_X^2) \quad (27)$$

in which $x_{.50}$ and V_X are the median and COV (coefficient of variation) of $X(t)$. Figures 6 and 7 show results for $V_X = 0.5$ and $V_X = 1.0$, for which (α_3, α_4) are (1.63, 8.04) and (4.00, 41.0), respectively. Findings here are similar to those in example 1. Even for the extremely non-Gaussian case when $V_X = 1.0$, a four-moment fit shows good accuracy to about $\nu(x)/\nu_0 = 10^{-3}$. In contrast, fits to four L-moments again begin to diverge from exact results at around $\nu(x)/\nu_0 = 10^{-2}$. (The four-moment fits here use “exact Hermite” models; i.e., Eq. (14) with c_3, c_4 chosen to give exact α_3, α_4 values.)

Maximum Entropy Models

Finally, we consider another model suggested for non-Gaussian processes: the “maximum entropy” model [6]. The resulting probability density of $X(t)$, assuming four moments are known, is of the form

$$f(x) = \exp[-\kappa(x)], \quad \kappa(x) = \sum_{n=0}^4 k_n x^n \quad (28)$$

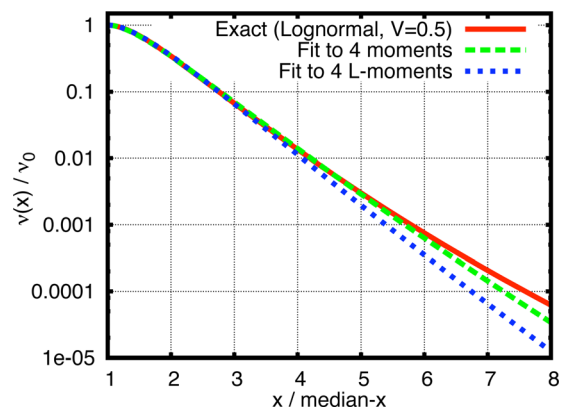


Fig. 6 Moments versus L-moments fits to a lognormal process with coefficient of variation $V_X = 0.5$

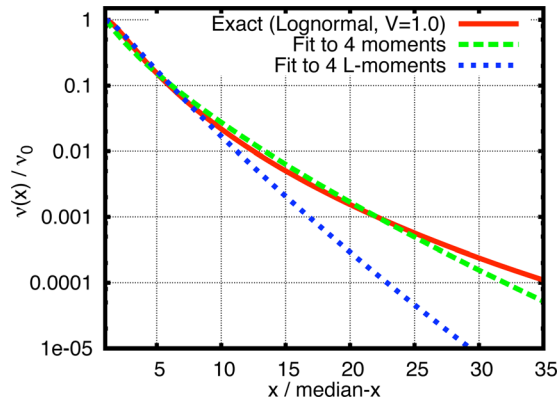


Fig. 7 Moments versus L-moments fits to a lognormal process with coefficient of variation $V_X = 1.0$

The coefficients k_1, \dots, k_4 are chosen to preserve (or minimize error in) the four moments. Unit area is achieved through k_0 .

Most critically, the behavior of Eq. (28) for large x is asymptotically given by its highest-order term. Thus, $f(x)$ will ultimately decay like $\exp(-k_4 x^4)$ as $|x| \rightarrow \infty$. This implies that

1. $k_4 \geq 0$ so that $f(x)$ converges as $|x| \rightarrow \infty$, and
2. Because $k_4 \geq 0$, $f(x)$ will ultimately decay *at least as fast as* the Gaussian density.

This makes the model of questionable use for “softening cases” ($\alpha_4 > 3$), the most common practical case of interest.

Example 1 Revisited. We first revisit example 1, for which we require that $f_X(x)$ be symmetric, hence $k_1 = k_3 = 0$. Because $k_4 \geq 0$, Eq. (28) must lead here to a “hardening” non-Gaussian model (with kurtosis $\alpha_4 \leq 3$). In fact, in this case Eq. (28) coincides with the exact result for a “Duffing oscillator,” which includes a cubic hardening spring. Because our example 1 cases require $\alpha_4 > 3$, there is no maximum entropy solution in these cases. (Of course, a “softening” model with $k_4 < 0$ can be forced if Eq. (28) is truncated at a finite upper-bound x_{\max} . However, all results will then depend upon the user-defined value of x_{\max} , required to reconcile the inappropriate functional form—hardening in Eq. (28)—with the actual softening behavior.)

Example 2 Revisited. We now revisit the lognormal cases in example 2. In contrast to example 1, the positive skewness values here yield negative k_3 in Eq. (28), which expands the right tail of $f_X(x)$ from the Gaussian model and hence can also give $\alpha_4 > 3$. However, as noted above we still require positive k_4 , so that these cases (and many others) yield (k_3, k_4) values of opposing signs. These opposing effects—and the resulting bimodal PDFs—are clearly shown in Figs. 8 and 9. PDF results begin to diverge from exact values when $f_X(x) / \max[f_X(x)]$ has fallen off to about 10^{-2} . Because $f_X(x)$ and $\nu(x)$ are roughly proportional—the proportionality is exact if X and \dot{X} are independent—this suggests that maximum entropy fails at a level similar to that of L-moment models. These failures, of course, have completely different causes: maximum entropy fails due to an inappropriate functional form, while L-moment models fail because their parameters are insufficiently tail sensitive.

Example 3. Because of its wide study in the literature (e.g., [8,9]), we consider a final case in which wind loads are applied to a 1DOF structure. The structural motion $X(t)$ satisfies

$$\ddot{X} + 2\zeta\omega_n\dot{X} + \omega_n^2 X = Y(t)^2 \quad (29)$$

in which $Y(t)$ is a normalized wind velocity process, assumed here to be a Gaussian process. Following the cited references, we

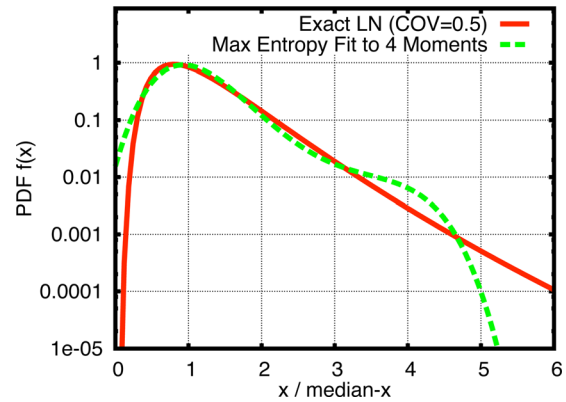


Fig. 8 Maximum entropy PDF models for a lognormal process with coefficient of variation $V_X = 0.5$

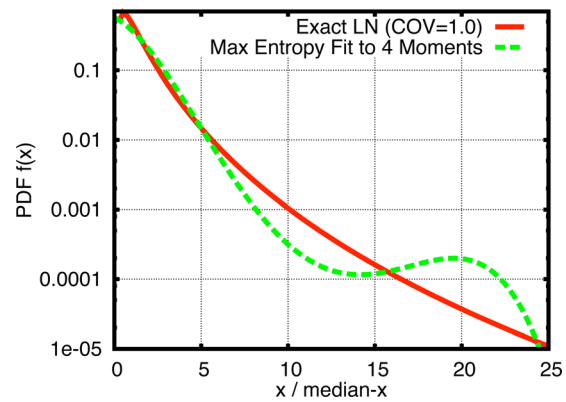


Fig. 9 Maximum entropy PDF models for a lognormal process with coefficient of variation $V_X = 1.0$

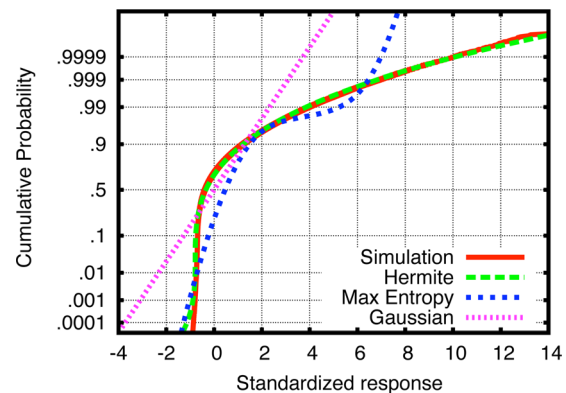


Fig. 10 Moment-fit versus maximum entropy models of the wind response of a 1DOF oscillator

assume here that $\omega_n = 1.26$ rad/s, $\zeta = 0.30$ (including viscous drag), and the covariance between $Y(t)$ and $Y(t + \tau)$ is $\exp(-0.12|\tau|)$. The response moments are then $\alpha_3 = 2.7$ and $\alpha_4 = 14.3$, suggesting notable non-Gaussian behavior.

Figure 10 shows the distribution of X , estimated by simulation, on normal probability scale. Also shown is a two-moment Gaussian fit, which, as may be expected, dramatically underestimates upper response fractiles of practical interest. The Hermite model (with exact four moments) is a marked improvement, showing good agreement far into the response tails. In contrast, the maximum entropy model is found inconsistent, due to its ultimate hardening nature noted above. It thus underestimates response fractiles

Table 2 Estimated 3-h extreme x_{3h} from different methods divided by exact value. All results assume $\nu(x_{3h})/\nu_0 = 10^{-3}$. Maximum entropy results also assume that $\nu(x)$ and $f(x)$ are proportional.

Exact model	Ratio of estimated to exact x_{3h} value			
	Nth order polynomial ($2 \leq N \leq 5$)		Lognormal	
Strength of nonlinearity	Moderate ($\alpha_4 = 5.0; \tau_4 = 0.185$)	Strong ($\alpha_4 = 7.0; \tau_4 = 0.220$)	Moderate (COV = 0.5)	Strong (COV = 1.0)
Hermite	0.94–1.07	0.95–1.08	0.98	1.00
L-Hermite	0.65–1.18	0.61–1.25	0.93	0.76
Max entropy	No solution available		1.01	0.79

x_p systematically for p above 0.999 (exceedance probabilities below 10^{-3}).

Summary

A range of non-Gaussian models have been surveyed. We first compare Hermite transformation models based on moments versus L-moments. While moment-based Hermite models are well-known, those based on L-moments are newly derived here.

Traditional four-moment models are shown to accurately estimate the response upcrossing rate $\nu(x)$ to levels of about $\nu(x)/\nu_0 = 10^{-3}$. (Here ν_0 is an “average” cycle rate; strictly, the upcrossing rate of the median of $X(t)$.) In contrast, models fit to four L-moments are not found to define the response tails with comparable accuracy. Different models with the same (τ_3, τ_4) are found to begin to diverge at around $\nu(x)/\nu_0 = 10^{-2}$.

The benefit of L-moments—their tail insensitivity—is also their weakness: model uncertainty here begins to arise an order of magnitude more frequently—at levels crossed every 100 cycles rather than 1000. Thus, in replacing moments by L-moments in the fitting, one trades statistical uncertainty (in moments) to model uncertainty (in the model’s tails given its relatively well-predicted L-moments). Because model uncertainty is relatively more difficult to quantify, this use of L-moments may not be beneficial.

Four-moment fits based on maximum entropy have also been considered (Eq. (28)). It is shown that the resulting functional form is generally inappropriate for softening ($\alpha_4 > 3$) cases, the situations of most common practical interest. This is because the maximum entropy functional form yields narrower-than-Gaussian tails in the upper limit. This mismatch is shown for a wind response example (Fig. 10), in which maximum entropy models underpredict exact results beyond about the $p = 0.999$ response fractile.

Table 2 summarizes the results of Figs. 2–9. It focuses on the maximum response x_{3h} in a 3-hour seastate. Assuming this seastate comprises 10^3 cycles, x_{3h} is defined here as $\nu(x_{3h})/\nu_0 = 10^{-3}$. For example, Fig. 2 shows that for a polynomial model with $\alpha_4 = 5.0$, exact values of x_{3h} range from $5.4\sigma_x$ to $6.2\sigma_x$ for $2 \leq n \leq 5$. Because the Hermite model predicts $5.8\sigma_x$, it leads to ratios of predicted/exact x_{3h} ratios of $5.8/(5.4–6.2)$ or $0.94–1.07$. The other values in this table are found similarly. The relative accuracy of the Hermite model seems clear.

Appendix: Fatigue Applications

For completeness we compare here fatigue damage estimates from moment and L-moment models. If Miner’s rule holds and $x(t)$ is narrow band, the expected damage $E[D]$ is proportional to $E[R^b]$, the expected b th moment of the stress range R . (Here b is a material property, which may be on the order of $2 \leq b \leq 5$ for welded steels and somewhat higher for some composite components. In particular, two-slope S-N curves, with $b = 3$ and 5 , are often used for steel offshore structures.)

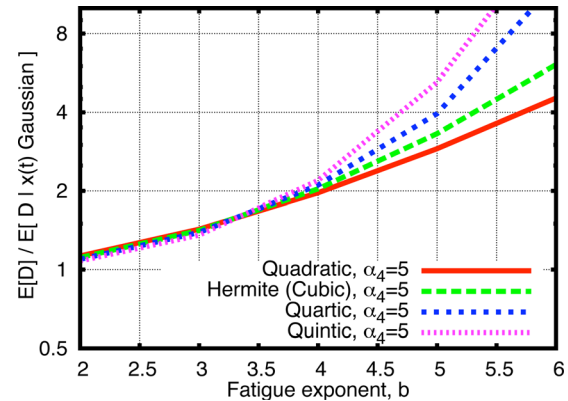


Fig. 11 Mean damage rates for various transformed Gaussian models, all calibrated to have kurtosis $\alpha_4 = 5$

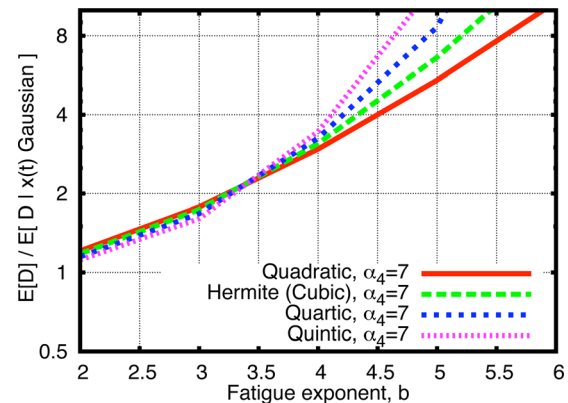


Fig. 12 Mean damage rates for various transformed Gaussian models, all calibrated to have kurtosis $\alpha_4 = 7$

If $x(t)$ is a standard narrow-band Gaussian process, R has Rayleigh distribution with moments

$$E[R^b] = \int_0^\infty (2u)^b u \exp(-u^2/2) du = (2\sqrt{2})^b \left(\frac{b}{2}\right)! \quad (A1)$$

If b is not an even integer, $(b/2)!$ should be interpreted as $\Gamma(1 + 0.5b)$.

We now consider non-Gaussian transformations, in which $x(t) = g[u(t)]$ in terms of a standard Gaussian process $u(t)$. Again assuming narrow-band behavior, the symmetric peaks of $u(t)$ at $S = R/2$ and $-S = -R/2$ are similarly transformed to yield a stress range

$$R_{NG} = g(S) - g(-S) \quad (A2)$$

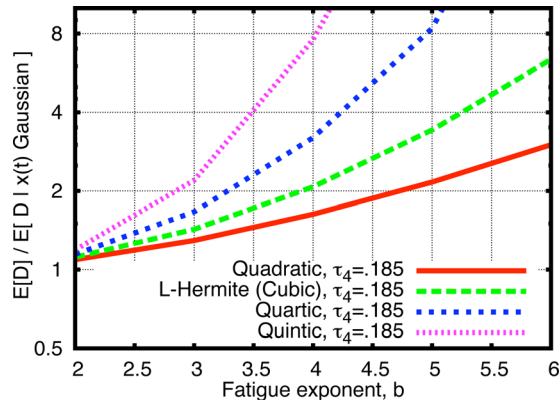


Fig. 13 Mean damage rates for various transformed Gaussian models, all calibrated to have L-kurtosis $\tau_4 = 0.185$

With the g function of example 1 (Eq. (25)), the Gaussian result in Eq. (A1) is replaced by

$$E[R_{NG}^b] = E[(2g(S))^b] = \int_0^\infty [2(u + cu^m)]^b u \exp(-u^2/2) du \quad (A3)$$

As expected, when $c=0$ this result reduces to Eq. (A1). More generally, Eq. (A3) can be evaluated numerically; e.g., transforming to $y = u^2/2$ and using Laguerre quadrature.

For integer b , the term $(u + cu^m)^b$ can be expanded as a series, and each integral term evaluated using Eq. (A1). This has been done here for $2 \leq b \leq 6$, and the results are shown in Figs. 11–14.

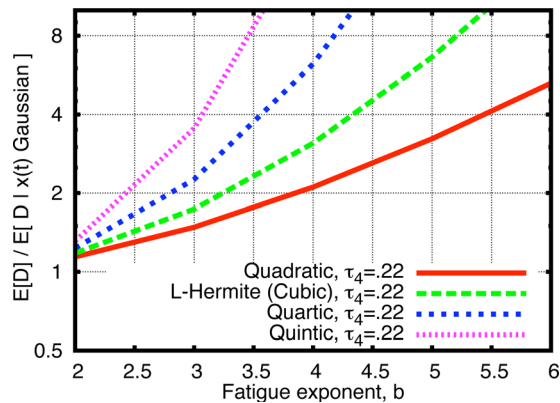


Fig. 14 Mean damage rates for various transformed Gaussian models, all calibrated to have L-kurtosis $\tau_4 = 0.220$

Specifically, these figures show a correction factor on fatigue damage over that predicted by a Gaussian model:

$$\frac{E[D]}{E[D|x(t)\text{Gaussian}]} = \frac{E[R_{NG}^b]}{(2\sqrt{2}\sigma_x)^b (b/2)!} \quad (A4)$$

Again, $E[R_{NG}^b]$ is found from Eq. (A3), which yields a closed-form result for integral b . The c values are found as described in example 1, calibrating Eq. (25) to have the desired α_4 or τ_4 value.

As may be expected from our previous findings, the moment-based results (Figs. 11 and 12) show little variability across models, particularly in the range $2 \leq b \leq 4$. In contrast, knowledge of L-moment values (Figs. 13 and 14) is not generally sufficient to accurately predict fatigue in these cases.

References

- [1] Hosking, J., 1990, "L-Moments: Analysis and Estimation of Distributions Using Linear Combinations of Order Statistics," *J. R. Stat. Soc. Ser. B*, **52**(1), pp. 105–124. Available at: <http://www.jstor.org/discover/10.2307/2345653?uid=3739560&uid=2&uid=4&uid=3739256&sid=47699115515527>
- [2] Izadparast, A., and Niedzwecki, J., 2009, "Probability Distributions for Wave Runup on Offshore Platform Columns," Proceedings of the 28th International Conference on Offshore Mechanics and Arctic Engineering, Honolulu, HI, May 31–June 5, ASME Paper No. OMAE2009-79625.
- [3] Najafian, G., 2010, "Comparison of Three Different Methods of Moments for Derivation of Probability Distribution Parameters," *Appl. Ocean Res.*, **32**(3), pp. 298–307.
- [4] Winterstein, S. R., 1988, "Nonlinear Vibration Models for Extremes and Fatigue," *J. Eng. Mech.*, **114**(10), pp. 1772–1790.
- [5] Kashef, T., and Winterstein, S. R., 2000, "Moment-Based Load and Response Models With Wind Engineering Applications," *ASME J. Solar Eng.*, **122**, pp. 122–128.
- [6] Jaynes, E., 1957, "Information Theory and Statistical Mechanics," *Phys. Rev.*, **106**, pp. 620–630.
- [7] Pandey, M., and Ariaratnam, S., 1996, "Crossing Rate Analysis of Non-Gaussian Response of Linear Systems," *J. Eng. Mech.*, **122**(6), pp. 507–511.
- [8] Kotulski, Z., and Sobczyk, K., 1981, "Linear Systems and Normality," *J. Stat. Phys.*, **24**(2), pp. 359–373.
- [9] Grigoriu, M., and Ariaratnam, S., 1987, "Stationary Response of Linear Systems to Non-Gaussian Excitations," Proceedings ICASP-5, Vancouver, Canada, May 25–29, Vol. 2, pp. 718–724.
- [10] MacKenzie, C. A., and Winterstein, S. R., 2011, "Comparing L-Moments and Conventional Moments to Model Current Speeds in the North Sea," Proceedings of the 2011 Industrial Engineering Research Conference, Inst. Industrial Eng. Annual Meeting, Reno, NV, May 21–25.
- [11] Winterstein, S. R., Lange, C. H., and Kumar, S., 1995, "FITTING: A Subroutine to Fit Four Moment Probability Distributions to Data," Technical Report SAND94-3039, Sandia National Laboratories.
- [12] Jensen, J. J., 1994, "Dynamic Amplification of Offshore Steel Platform Responses Due to Non-Gaussian Wave Loads," *Marine Struct.*, **7**(1), pp. 91–105.
- [13] Yang, L., Gurley, K. R., and Prevatt, D. O., 2011, "Probabilistic Modeling of Wind Pressure on Low-Rise Buildings," *J. Wind Eng. Ind. Aerodyn.* (submitted). Abridged version in Proceedings of the 13th International Conference on Wind Engineering (ICWE13), Amsterdam, July 10–15.
- [14] Winterstein, S. R., and MacKenzie, C. A., 2011, "Extremes of Nonlinear Vibration: Models Based on Moments, L-Moments, and Maximum Entropy," Proceedings of the 30th International Conference on Offshore Mechanics and Arctic Engineering, Rotterdam, The Netherlands, June 19–24, ASME Paper No. OMAE2011-49867.